






Magnetization process of the insulating ferromagnetic semiconductor (Al,Fe)Sb

Shoya Sakamoto ¹, Le Duc Anh ^{2,3}, Pham Nam Hai ^{4,2,5}, Yukiharu Takeda,⁶ Masaki Kobayashi,^{2,5} Yuki K. Wakabayashi,² Yosuke Nonaka,¹ Keisuke Ikeda,¹ Zhendong Chi,¹ Yuxuan Wan,¹ Masahiro Suzuki,¹ Yuji Saitoh,⁶ Hiroshi Yamagami,^{6,7} Masaaki Tanaka ^{2,5} and Atsushi Fujimori ^{1,6}

¹*Department of Physics, The University of Tokyo, Bunkyo-ku, Tokyo 113-0033, Japan*

²*Department of Electrical Engineering and Information Systems, The University of Tokyo, Bunkyo-ku, Tokyo 113-8656, Japan*

³*Institute of Engineering Innovation, The University of Tokyo, Bunkyo-ku, Tokyo 133-8656, Japan*

⁴*Department of Electrical and Electronic Engineering, Tokyo Institute of Technology, Meguro-ku, Tokyo 152-0033, Japan*

⁵*Center for Spintronics Research Network (CSRN), The University of Tokyo, Bunkyo-ku, Tokyo 113-8656, Japan*

⁶*Materials Sciences Research Center, Japan Atomic Energy Agency (JAEA), Sayo-gun, Hyogo 679-5148, Japan*

⁷*Department of Physics, Kyoto Sangyo University, Kyoto 603-8555, Japan*



(Received 11 February 2019; revised manuscript received 17 October 2019; accepted 27 January 2020; published 13 February 2020; corrected 12 May 2020)

We have studied the magnetization process of the new insulating ferromagnetic semiconductor (Al,Fe)Sb by means of x-ray magnetic circular dichroism. For an optimally doped sample with 10% Fe, a magnetization was found to rapidly increase at low magnetic fields and to saturate at high magnetic fields at room temperature, well above the Curie temperature of 40 K. We attribute this behavior to the existence of nanoscale Fe-rich ferromagnetic domains acting as superparamagnets. By fitting the magnetization curves using the Langevin function representing superparamagnetism plus the paramagnetic linear function, we estimated the average magnetic moment of the nanoscale ferromagnetic domain to be $300\mu_B - 400\mu_B$ and the fraction of Fe atoms participating in the nanoscale ferromagnetism to be $\sim 50\%$. Such behavior was also reported for (In,Fe)As:Be and Ge:Fe and seems to be a universal characteristic of the Fe-doped ferromagnetic semiconductors. Further Fe doping up to 14% led to the weakening of the ferromagnetism, probably because antiferromagnetic superexchange interaction between nearest-neighbor Fe-Fe pairs becomes dominant.

DOI: [10.1103/PhysRevB.101.075204](https://doi.org/10.1103/PhysRevB.101.075204)

I. INTRODUCTION

Recently, Fe-doped ferromagnetic semiconductors (FMSs) were synthesized and have attracted much attention owing to their high Curie temperatures T_C and distinct properties compared to the prototypical Mn-doped systems. First, the T_C 's are higher than room temperature: 340 K for (Ga,Fe)Sb [1] and 335 K for (In,Fe)Sb [2], while that of (Ga,Mn)As is, at most, 200 K [3]. Second, various types of transport properties are realized: p type for (Ga,Fe)Sb [4] and Ge:Fe [5], n type for (In,Fe)As [6] and (In,Fe)Sb [2], and insulating for (Al,Fe)Sb [7], while only p type is possible for Mn-doped III-V group semiconductors. Furthermore, in the case of (In,Fe)As, a large Curie temperature modulation of 42% was demonstrated by wave function engineering in field-effect transistor structures [8], and the spin splitting of the conduction band bottom was observed in Esaki-diode structures [9]. Despite the attractive properties, however, the origin of ferromagnetism is unclear and remains to be investigated.

In the insulating FMS (Al,Fe)Sb, ferromagnetism of $T_C = 40$ K emerges for 10% of Fe doping, and the hole concentration is about 10^{17} cm^{-3} [7]. Unlike the other FMSs, further Fe doping up to 14% leads to the decrease in T_C down to 10 K, and the two orders of magnitudes increase in the hole concentration up to 10^{19} cm^{-3} . This is probably because the crystal quality is degraded through the creation of a high concentration of defects, although there is no clear signature

of phase separation from reflection high-energy electron-diffraction patterns and x-ray diffraction profiles.

Since (Al,Fe)Sb is insulating, the ferromagnetism is most likely not carrier induced, being different from the other typical FMSs [10]. In the present study, for the purpose of revealing the mechanism of how ferromagnetism appears in (Al,Fe)Sb, we have conducted x-ray absorption spectroscopy (XAS) and x-ray magnetic circular dichroism (XMCD) measurements at the Fe $L_{2,3}$ absorption edges. XAS and XMCD are powerful methods to investigate the magnetism as well as the local electronic structure of specific elements and have been used for studies of magnetic semiconductors [11,12]. Since XAS and XMCD are element-specific probes, one can eliminate the diamagnetic component from the substrate, which is usually dominant in the case of diluted magnetic materials in the thin-film form. One can thus precisely estimate the paramagnetic (PM) linear component as well as the ferromagnetic (FM) component from magnetization curves [13].

In the previous XMCD study on (In,Fe)As:Be [13] and Ge:Fe [14], it was found that nano-scale FM domains exist far above the Curie temperature. On lowering the temperature, those domains seemed to coalesce, resulting in global ferromagnetism at the Curie temperature. In the present study, we have found the same behavior for (Al,Fe)Sb and concluded that the nanoscale FM domains of several hundreds of μ_B are formed in Fe-rich regions, which is likely the universal feature of Fe-doped magnetic semiconductors.

II. EXPERIMENT

Two samples, $\text{Al}_{0.9}\text{Fe}_{0.1}\text{Sb}$ and $\text{Al}_{0.86}\text{Fe}_{0.14}\text{Sb}$, were grown using low-temperature molecular beam epitaxy methods. The structure of the samples was, from the top surface to the bottom, InAs cap (5 nm)/(Al,Fe)Sb (100 nm)/AlSb (100 nm)/GaAs (100 nm)/*p*-GaAs(001) substrate. The details of the sample growth are described in Ref. [7]. The T_C 's were estimated to be about 40 and 10 K for the 10% and 14% Fe-doped samples, respectively, from the Arrott plots of the visible-light magnetic circular dichroism intensity [15]. The XAS and XMCD experiments were conducted at beamline BL23SU of SPring-8. Measurement temperature T was varied from 5.8 to 300 K, and magnetic field $\mu_0 H$ was varied from -7 to 7 T. The samples were placed in the measurement chamber so that the sample surface was perpendicular to the x-ray incident direction and hence the magnetic field. Absorption signals were collected in the total electron yield mode, and dichroic signals were measured by reversing the helicity of x rays with 1-Hz frequency at each photon energy. The spectra were obtained by sweeping the photon energy under a fixed magnetic field, and the scans were repeated with the opposite magnetic field direction to minimize experimental artifacts. That is, each XMCD spectrum was obtained as $(\sigma_{+,h} - \sigma_{-,h}) + (\sigma_{-,-h} - \sigma_{+,-h})$, and each XAS spectrum was obtained as the summation of all four terms, where σ denotes the absorption cross sections, the first subscript is the helicity of the x rays, and the second subscript is the direction of the magnetic field. We also measured magnetization curves by recording XMCD signals at photon energies of the $L_{2,3}$ edges while sweeping the magnetic field. The data have been normalized to the total magnetic moment at $\mu_0 H = 7$ T deduced by applying the XMCD sum rules to the spectra [16–18].

III. RESULTS AND DISCUSSION

Figure 1(a) shows raw absorption spectra of the 10% Fe-doped sample taken with x rays of positive and negative helicities under $\mu_0 H = 7$ T and $T = 5.8$ K. A large difference between the spectra taken with different helicities indicates that the magnetism indeed arises from the Fe atoms. Because there was a 5-nm-thick InAs capping layer to prevent oxidation, a relatively strong In M_2 peak overlapped the Fe L_3 peak. In order to remove the In contribution, we assumed a Lorentzian function and subtracted it from the spectra together with a linear background. Double step functions representing the Fe $L_{2,3}$ -edge jumps have also been subtracted. The summation and the difference spectra of the different helicities after the background subtraction are shown at the bottom of Fig. 1(a). Note that we have processed all the data in the same manner.

Figures 1(b) and 1(c) show the magnetic field dependence of the XAS and XMCD spectra of the 10% Fe-doped sample recorded at 5.8 K. Here, each spectrum was obtained as an average of the spectra taken under two opposite magnetic field directions as described in Sec. II and was normalized to unity. It can be seen that the spectral line shapes are almost identical to each other, suggesting that there is no second phase in this system.

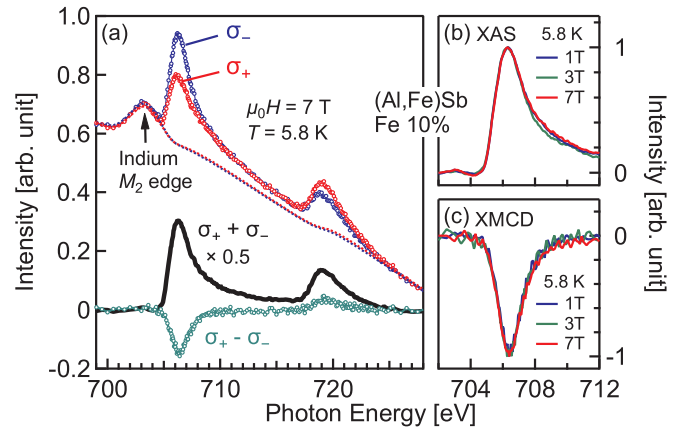


FIG. 1. (a) Absorption spectra taken with x rays of positive and negative helicities. Dashed curves at the top represent the backgrounds, which consist of a Lorentzian function representing the indium M_2 peak, a double-step function for edge jumps, and a linear function. At the bottom, XAS and XMCD spectra after the background subtraction are also shown. (b) and (c) Magnetic field dependences of the line shapes of XAS and XMCD spectra normalized to unity.

Figure 2 compares the XAS and XMCD spectra of (Al,Fe)Sb with those of the other Fe-doped FMSSs, namely, (Ga,Fe)Sb and (In,Fe)As:Be, Fe metal, FeCr_2S_4 (Fe^{2+}), and Fe_2O_3 (Fe^{3+}). The XAS and XMCD spectra of (Al,Fe)Sb are broad and asymmetric, having a tail on the high-energy side, similar to the case of Fe metal. In addition, fine structures due to multiplet splitting are hardly seen but would be present if the Fe $3d$ electrons were localized as in Fe_2O_3 and FeCr_2S_4 . Such an asymmetric line shape without mul-

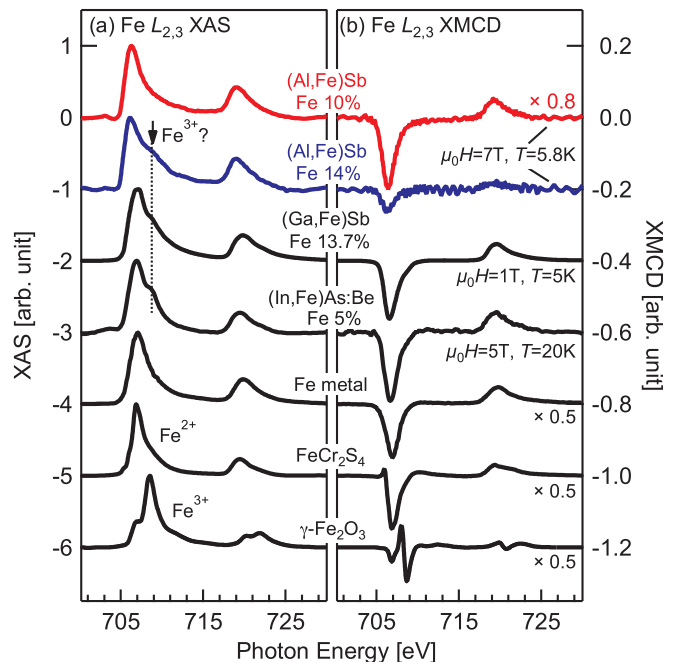


FIG. 2. XAS and XMCD spectra of (Al,Fe)Sb in comparison with those of (Ga,Fe)Sb [19], (In,Fe)As:Be [13], Fe metal [18], FeCr_2S_4 , and $\gamma\text{-Fe}_2\text{O}_3$ [20].

triplet features indicate the significant delocalization of the Fe 3*d* electrons and would challenge the assumption that Fe takes the valence of 3+ with localized five 3*d* electrons. The same is also true for the other Fe-doped FMSs [13,14], and the itinerancy of Fe 3*d* electrons seems to be a key for the ferromagnetism of the Fe-doped systems. Furthermore, the XMCD spectra of (Al,Fe)Sb, (Ga,Fe)Sb, and (In,Fe)As:Be have almost identical line shapes, indicating that the local electronic structure of the Fe atoms that contribute to the ferromagnetism is similar among the Fe-doped FMSs. Note that the shoulders around 709 eV that the XAS spectra of (Ga,Fe)Sb and (In,Fe)As:Be have been attributed to Fe³⁺ signals originating from Fe oxides formed near the sample surfaces [13,21] because a corresponding feature does not exist in the XMCD spectra. The XAS spectrum of the 14% Fe-doped AlSb also exhibits such a shoulder, which may be either due to the existence of surface oxides as in the cases of (Ga,Fe)Sb and (In,Fe)As:Be or due to some defect states considering the lower crystal quality of the 14% Fe-doped AlSb sample lower than the 10% Fe-doped one. The shoulder occupies ~17% of the area of the XAS spectrum [15].

The XMCD intensity is considerably weaker for the 14% Fe-doped sample than for the 10% Fe-doped sample, consistent with the observation that the Curie temperature decreases with increasing Fe concentration from 10% to 14%. This also suggests that the ferromagnetism of (Al,Fe)Sb is not due to Fe-metal precipitates or any second phases because if the magnetism originated from Fe-metal precipitates, a higher Fe doping level would result in enhanced ferromagnetism. Considering that the spectral line shapes of XAS and XMCD are similar between the two samples except for the smaller shoulder in the XAS spectrum of the 14% Fe-doped sample, the disappearance or the weakening of the ferromagnetism with increasing Fe concentration also seems intrinsic.

The spin and orbital magnetic moments at $\mu_0 H = 7$ T and $T = 5.8$ K estimated from the XMCD sum rules were $(m_{\text{spin}}, m_{\text{orb}}) = (1.6\mu_B, 0.4\mu_B)$ for the 10% Fe-doped sample and $(0.5\mu_B, 0.1\mu_B)$ for the 14% Fe-doped one. Here, we have assumed the number of 3*d* electrons to be six, which was deduced from first-principles supercell calculations [22], and the correction factor [23] to be 0.875 for the Fe²⁺ state [24,25]. The spin and orbital magnetic moments of the 14% Fe-doped sample were multiplied by $1/(1 - 0.17)$ in order to remove the contribution from the shoulder feature in the XAS spectrum [15]. The unquenched orbital magnetic moments seem to support the mixture of the 3*d*⁶ \underline{L} configuration of the Fe atom, where \underline{L} denotes a ligand hole, because there is no orbital degree of freedom for the high-spin *d*⁵ state. Note that the uncertainty in $m_{\text{orb}}/m_{\text{spin}}$ and $m_{\text{orb}} + m_{\text{spin}}$ can be as large as ~20% and ~10%, respectively, because the thick InAs capping layer made signals very weak.

Figures 3(a) and 3(b) show the magnetization curves at various temperatures measured by XMCD. Here, hysteresis was not detected because it was too small. Despite the fact that the T_C below which hysteresis appears is as low as 40 K for the 10% Fe-doped sample, the relatively large magnetization M is induced by the magnetic field even at 300 K in contrast to typical ferromagnets, where magnetization disappears rather quickly above T_C . We attribute this behavior to the superparamagnetism of nanoscale FM domains, as has been found

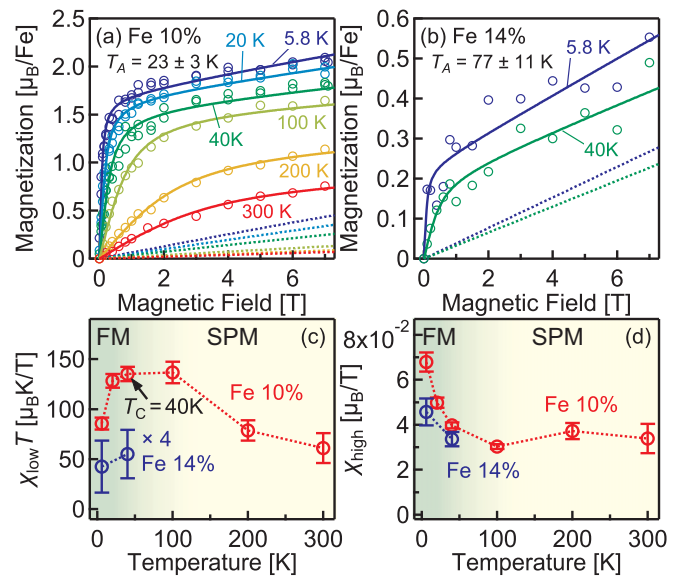


FIG. 3. (a) Magnetization curves of the 10% Fe-doped sample and (b) the 14% Fe-doped sample deduced from XMCD. The fitting results are shown by solid curves, and the linear PM components are also shown separately by dashed lines. (c) Magnetic susceptibility at low magnetic fields near 0 T χ_{low} [defined by Eq. (1)] and (d) that at high magnetic fields around 7 T χ_{high} [also defined by Eq. (1)], which have been deduced from the fitting. Here, χ_{low} is multiplied by temperature, and $\chi_{\text{low}}T$ of the 14% Fe-doped sample is multiplied by 4 for a better visualization.

in other Fe-doped FMSs [13,14]. At the low temperature of 5.8 K, the magnetization at high magnetic fields shows a gradual linear increase after the steep increase at low magnetic fields. This indicates the existence of PM Fe atoms even below T_C .

To be quantitative, the magnetic susceptibilities or the slopes of the magnetization versus magnetic field curve at low and high magnetic fields,

$$\chi_{\text{low}} = \left. \frac{\Delta M}{\Delta(\mu_0 H)} \right|_{\mu_0 H=0T}, \quad \chi_{\text{high}} = \left. \frac{\Delta M}{\Delta(\mu_0 H)} \right|_{\mu_0 H=7T}, \quad (1)$$

are plotted in Figs. 3(c) and 3(d), respectively. Note that in Fig. 3(c), χ_{low} is multiplied by the temperature to see whether χ_{low} is inversely proportional to temperature as in ideal superparamagnets. Although $\chi_{\text{low}}T$ of the 10% Fe-doped sample shows some temperature dependence, it remains large even at 300 K. This again indicates the existence of superparamagnetism. On lowering the temperature, $\chi_{\text{low}}T$ gradually increases, probably because the number of Fe atoms participating in superparamagnetism increases. Further lowering the temperature down to below $T_C = 40$ K leads to a drop in $\chi_{\text{low}}T$. This implies that the system turns into global ferromagnetism, which cannot be explained by superparamagnetism.

The finite χ_{high} at the low temperature of 5.8 K indicates the coexistence of ferromagnetism and paramagnetism as mentioned above. The values are comparable between the two samples, although χ_{high} of the sample with 14% Fe could be much larger than that of the sample with 10% Fe considering that there are many more PM Fe atoms. This behavior can

be understood if a large fraction of Fe atoms is coupled antiferromagnetically in the 14% Fe-doped sample.

In order to understand the behavior of χ_{low} and χ_{high} and how the PM and superparamagnetic (SPM)/FM phase coexist in more detail, we fitted the linear combination of the Langevin function $L(\xi)$ representing superparamagnetism and a linear function representing paramagnetism to the data:

$$M = xm_{\text{sat}}L\left(\frac{\mu\mu_0H}{k_B T}\right) + (1-x)\frac{C\mu_0H}{T+T_A}, \quad (2)$$

$$C = \frac{m_{\text{sat}}(m_{\text{sat}} + 2\mu_B)}{3k_B}, \quad (3)$$

$$L(\xi) = \coth(\xi) - \frac{1}{\xi}, \quad (4)$$

where M is the magnetization per Fe atom, m_{sat} is the total magnetic moment of the Fe atom, k_B is the Boltzmann constant, and C is the Curie constant. We have assumed that $m_{\text{sat}} = 3.4\mu_B$, which was obtained by the first-principles supercell calculation, and that the g factor is 2 for simplicity. Fitting parameters in the present model are the following: μ is the total magnetic moment of a nanoscale FM domain, x is the fraction of Fe atoms participating in ferromagnetism or superparamagnetism, and T_A is the antiferromagnetic Weiss temperature. Here, μ and x were allowed to vary with temperature, while T_A was kept constant. The relationship between Eqs. (1) and (2) is shown in the Supplemental Material [15]. Note that there is almost no magnetic anisotropy in (Al,Fe)Sb [26], probably due to its cubic zinc-blende crystal structure, and the fitting results would not be affected.

The fitted curves are shown by solid curves, and the linear PM components are separately shown by dashed lines in Figs. 3(a) and 3(b). As can be seen, the data were fitted well by Eqs. (2)–(4). The fit yielded an antiferromagnetic Weiss temperature of 23 K for the sample with 10% Fe and 77 K for the sample with 14% Fe, again indicating that antiferromagnetic correlations are stronger for the sample with 14% Fe. This may be because antiferromagnetic superexchange interactions between adjacent Fe atoms become dominant when the concentration of doped Fe atoms increases. Similar Weiss temperatures of ~ 30 K were reported for paramagnetic diluted magnetic semiconductors such as (Zn,Mn)Te [27] and (Ga,Fe)As [28] and for the ferromagnetic semiconductor (Ga,Mn)As [11]. Note that using the Brillouin function instead of a linear function does not change the line shape of the fitting curves as well as the fitting parameters because relatively large Weiss temperatures make the Brillouin function linear within the range of 0 to 7 T even at the lowest temperature of 5.8 K.

Figures 4(a) and 4(b) show the temperature dependences of the obtained fitting parameters x , the fraction of Fe atoms participating in ferromagnetism or superparamagnetism, and μ , the total magnetic moment of each nanoscale FM domain, respectively. x for the sample with 14% Fe was only about 5%, which confirms the near absence of ferromagnetism in the sample with 14% Fe. In the case of the 10% Fe-doped sample, 25% of Fe atoms still contribute to the ferromagnetism or superparamagnetism at 300 K. With decreasing temperature, x gradually increases, while 50% Fe remain PM at 5.8 K. These observations highlight the inhomogeneous

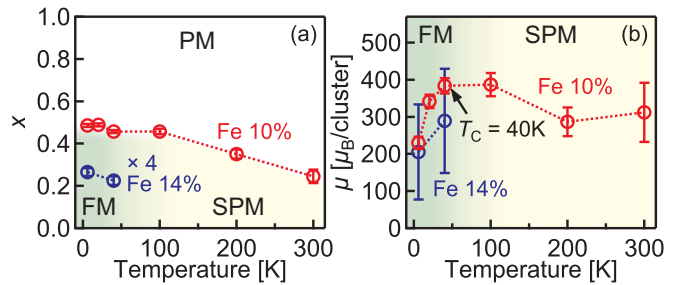


FIG. 4. Fitting parameters. (a) Fraction of Fe atoms contributing to ferromagnetism or superparamagnetism, denoted by x . Here, x of the 14% Fe-doped sample is multiplied by 4. (b) Total magnetic moment μ per nanoscale FM domain.

nature of magnetism in (Al,Fe)Sb. The magnetic moment per nanoscale FM domain was found to be $300\mu_B - 400\mu_B$ and increased from $\sim 300\mu_B$ to $\sim 400\mu_B$ with decreasing temperature from 300 to 40 K. Note that μ dropped suddenly below 40 K, as $\chi_{\text{low}}T$ dropped, reflecting the gradual appearance of macroscopic ferromagnetism and concomitant deviation from the Langevin behavior. Such a SPM response from the nanoscale FM domains with several hundreds of μ_B was also reported for (In,Fe)As:Be [13] and Ge:Fe [14] and seems to be a universal feature of the Fe-doped FMSs. Here, μ of $300\mu_B - 400\mu_B$ corresponds to $\mu/m_{\text{Fe}} \sim 100$ Fe atoms. The density of nanoscale FM domains can be deduced from μ and x as $7 \times 10^{18} \text{ cm}^{-3}$ for the 10% Fe-doped sample and $2 \times 10^{18} \text{ cm}^{-3}$ for the 14% Fe-doped sample.

The origin of the nanoscale FM domains can be attributed to the nanoscale fluctuation of Fe distribution as discussed for the other Fe-doped semiconductors (In,Fe)As:Be [13,29,30] and Ge:Fe [14,31,32]. In addition, the previous theoretical studies where chemical pair interactions were calculated suggested that Fe atoms tend to segregate and form Fe-rich regions in the InAs [29] and Ge [31] matrices while maintaining the zinc-blende and diamond lattice structures. The same kind of scenario is likely to apply to (Al,Fe)Sb and possibly to the other Fe-doped FMSs. If so, FM interaction between Fe $3d$ orbitals can stabilize the ferromagnetism in nanoscale Fe-rich FM domains at rather high temperatures up to 300 K. This is consistent with the present XAS and XMCD spectra, where rather close Fe-Fe distance bestows the itinerancy of the $3d$ electrons. On lowering the temperature, those domains would start to overlap or interact with each other, resulting in the macroscopic ferromagnetism.

IV. SUMMARY

We have performed x-ray absorption spectroscopy and x-ray magnetic circular dichroism on the new ferromagnetic semiconductor (Al,Fe)Sb to study its electronic structure and magnetization process. The spectral line shapes were broad and asymmetric, having a tail on the high-energy side, indicating the itinerant nature of Fe $3d$ electrons. The XMCD sum rules yielded an unquenched orbital magnetic moment, which suggests that a considerable fraction of Fe atoms takes the $3d^6$ configuration with a ligand hole. From the magnetization curves measured by XMCD, we have found that nanoscale ferromagnetic domains of $300\mu_B - 400\mu_B$ exist even at room

temperature in the optimally doped sample with 10% Fe ($T_C = 40$ K), and the system behaves as a superparamagnet. The formation of such domains was ascribed to the nonuniform distribution of Fe atoms on the nanoscale, which appears to be a common characteristics of the other Fe-doped FMSs. For the 14% Fe-doped sample, the weakening of the ferromagnetism and the strengthening of the antiferromagnetic correlations were observed compared to the 10% Fe-doped sample. This may be because antiferromagnetic superexchange interaction between adjacent Fe atoms becomes dominant when the system is doped with a large concentration of Fe atoms.

ACKNOWLEDGMENTS

This work was supported by Grants-in-Aids for Scientific Research from JSPS (Grants No. 15H02109 and No.

17H04922). The experiment was done under the Shared Use Program of JAEA Facilities (Proposals No. 2016B-E20 and No. 2017A-E20) with the approval of the Nanotechnology Platform Project supported by MEXT (Proposals No. A-16-AE-0030 and No. A-17-AE-0018). The synchrotron radiation experiments were performed at the JAEA beamline BL23SU in SPring-8 (Proposals No. 2016B3841 and No. 2017A3841). A.F. acknowledges support as an adjunct member of the Center for Spintronics Research Network (CSRN), the University of Tokyo, under the Spintronics Research Network of Japan (Spin-RNJ). S.S. acknowledges financial support from the Advanced Leading Graduate Course for Photon Science (ALPS) and the JSPS Research Fellowship for Young Scientists. Z.C. acknowledges financial support from the Materials Education Program for the Futures Leaders in Research, Industry, and Technology (MERIT).

- [1] N. T. Tu, P. N. Hai, L. D. Anh, and M. Tanaka, *Appl. Phys. Lett.* **108**, 192401 (2016).
- [2] N. T. Tu, P. N. Hai, L. D. Anh, and M. Tanaka, *Appl. Phys. Express* **11**, 063005 (2018).
- [3] L. Chen, X. Yang, F. Yang, J. Zhao, J. Misuraca, P. Xiong, and S. von Molnár, *Nano Lett.* **11**, 2584 (2011).
- [4] N. T. Tu, P. N. Hai, L. D. Anh, and M. Tanaka, *Phys. Rev. B* **92**, 144403 (2015).
- [5] Y. K. Wakabayashi, Y. Ban, S. Ohya, and M. Tanaka, *Phys. Rev. B* **90**, 205209 (2014).
- [6] P. Nam Hai, L. Duc Anh, S. Mohan, T. Tamegai, M. Kodzuka, T. Ohkubo, K. Hono, and M. Tanaka, *Appl. Phys. Lett.* **101**, 182403 (2012).
- [7] L. D. Anh, D. Kaneko, P. N. Hai, and M. Tanaka, *Appl. Phys. Lett.* **107**, 232405 (2015).
- [8] L. D. Anh, P. N. Hai, Y. Kasahara, Y. Iwasa, and M. Tanaka, *Phys. Rev. B* **92**, 161201(R) (2015).
- [9] L. D. Anh, P. N. Hai, and M. Tanaka, *Nat. Commun.* **7**, 13810 (2016).
- [10] T. Dietl and H. Ohno, *Rev. Mod. Phys.* **86**, 187 (2014).
- [11] K. W. Edmonds, N. R. S. Farley, T. K. Johal, G. van der Laan, R. P. Campion, B. L. Gallagher, and C. T. Foxon, *Phys. Rev. B* **71**, 064418 (2005).
- [12] Y. Takeda, M. Kobayashi, T. Okane, T. Ohkochi, J. Okamoto, Y. Saitoh, K. Kobayashi, H. Yamagami, A. Fujimori, A. Tanaka, J. Okabayashi, M. Oshima, S. Ohya, P. N. Hai, and M. Tanaka, *Phys. Rev. Lett.* **100**, 247202 (2008).
- [13] S. Sakamoto, L. D. Anh, P. N. Hai, G. Shibata, Y. Takeda, M. Kobayashi, Y. Takahashi, T. Koide, M. Tanaka, and A. Fujimori, *Phys. Rev. B* **93**, 035203 (2016).
- [14] Y. K. Wakabayashi, S. Sakamoto, Y.-h. Takeda, K. Ishigami, Y. Takahashi, Y. Saitoh, H. Yamagami, A. Fujimori, M. Tanaka, and S. Ohya, *Sci. Rep.* **6**, 23295 (2016).
- [15] See Supplemental Material at <http://link.aps.org/supplemental/10.1103/PhysRevB.101.075204> for an estimation of the Curie temperature using the Arrott plots of visible-light and x-ray magnetic circular dichroism intensities, x-ray absorption spectrum decomposition, and the relationship between the magnetic susceptibilities and the fitting parameters.
- [16] B. T. Thole, P. Carra, F. Sette, and G. van der Laan, *Phys. Rev. Lett.* **68**, 1943 (1992).
- [17] P. Carra, B. T. Thole, M. Altarelli, and X. Wang, *Phys. Rev. Lett.* **70**, 694 (1993).
- [18] C. T. Chen, Y. U. Idzerda, H.-J. Lin, N. V. Smith, G. Meigs, E. Chaban, G. H. Ho, E. Pellegrin, and F. Sette, *Phys. Rev. Lett.* **75**, 152 (1995).
- [19] V. K. Verma, V. R. Singh, K. Ishigami, G. Shibata, T. Harano, T. Kadono, A. Fujimori, T. Koide, K. Ohgushi, and Y. Tokura, *Photon Fact. Ac. Rep.* **29**, 129 (2012).
- [20] S. Brice-Profeta, M.-A. Arrio, E. Tronc, N. Menguy, I. Letard, C. C. dit Moulin, M. Noguès, C. Chanéac, J.-P. Jolivet, and P. Saintavrit, *J. Magn. Magn. Mater.* **288**, 354 (2005).
- [21] S. Sakamoto, N. T. Tu, Y. Takeda, S.-i. Fujimori, P. N. Hai, L. D. Anh, Y. K. Wakabayashi, G. Shibata, M. Horio, K. Ikeda, Y. Saitoh, H. Yamagami, M. Tanaka, and A. Fujimori, *Phys. Rev. B* **100**, 035204 (2019).
- [22] S. Sakamoto and A. Fujimori, *J. Appl. Phys.* **126**, 173910 (2019).
- [23] The correction factor is defined as the ratio of the spin magnetic moment obtained by the spin sum rule to the actual spin magnetic moment.
- [24] Y. Teramura, A. Tanaka, and T. Jo, *J. Phys. Soc. Jpn.* **65**, 1053 (1996).
- [25] C. Piamonteze, P. Miedema, and F. M. F. de Groot, *Phys. Rev. B* **80**, 184410 (2009).
- [26] L. D. Anh, P. N. Hai, and M. Tanaka (unpublished).
- [27] Y. Shapira, S. Foner, P. Becla, D. N. Domingues, M. J. Naughton, and J. S. Brooks, *Phys. Rev. B* **33**, 356 (1986).
- [28] S. Haneda, M. Yamaura, Y. Takatani, K. Hara, S. Harigae, and H. Munekata, *Jpn. J. Appl. Phys.* **39**, L9 (2000).
- [29] N. D. Vu, T. Fukushima, K. Sato, and H. Katayama-Yoshida, *Jpn. J. Appl. Phys.* **53**, 110307 (2014).

- [30] Y. Yuan, R. Hübner, M. Birowska, C. Xu, M. Wang, S. Prucnal, R. Jakiela, K. Potzger, R. Böttger, S. Facsko, J. A. Majewski, M. Helm, M. Sawicki, S. Zhou, and T. Dietl, *Phys. Rev. Materials* **2**, 114601 (2018).
- [31] H. Shinya, T. Fukushima, A. Masago, K. Sato, and H. Katayama-Yoshida, *Phys. Rev. B* **96**, 104415 (2017).
- [32] S. Sakamoto, Y. K. Wakabayashi, Y. Takeda, S.-i. Fujimori, H. Suzuki, Y. Ban, H. Yamagami, M. Tanaka, S. Ohya, and A. Fujimori, *Phys. Rev. B* **95**, 075203 (2017).

Correction: The order of authors has been modified, and the affiliations are now identified by superscript numbers. A second affiliation has been added for the last author.